

Amino Functionalized Zeolitic Tetrazolate Framework with High Capacity for Storage of Carbon Dioxide

(Supporting Information: 30 pages including this page)

Tamas Panda, Pradip Pachfule, Yifei Chen, Jianwen Jiang, and Rahul Banerjee*

Physical/Materials Chemistry Division, National Chemical Laboratory, Dr. Homi Bhaba Road, Pune- 411008, India; Department of Chemical & Biomolecular Engineering, National University of Singapore, 117576, Singapore

E-mail: r.banerjee@ncl.res.in Fax: + 91-20-25902636; Tel: + 91-20-25902535

Section S1. Detailed synthesis procedures for MOFs	S-2
Section S2. Single crystal X-ray diffraction data collection, structure solution and refinement procedures	S-9
Section S3. Thermal stability of MOFs and TGA data	S-17
Section S4. Gas adsorption analysis of Amino Tetrazole MOF	S-19
Section S5. Computational studies	S-24

Section S1: Detailed synthesis procedures for Amino Tetrazole MOFs including multi-gram scale synthesis, experimental and simulated PXRD patterns

All reagents and solvents for synthesis and analysis were commercially available and used as received. The Fourier transform (FT) IR spectra (KBr pellet) were taken on a *PERKIN ELMER FT-IR SPECTRUM* (Nicolet) spectrometer. Powder X-ray diffraction (PXRD) patterns were recorded on a Phillips PANalytical diffractometer for Cu K α radiation ($\lambda = 1.5406 \text{ \AA}$), with a scan speed of 2° min^{-1} and a step size of 0.02° in 2θ . Thermo-gravimetric experiments (TGA) were carried out in the temperature range of 25–800 °C on a SDT Q600 TG-DTA analyzer under N₂ atmosphere at a heating rate of $10^\circ \text{ C min}^{-1}$.

Thionyl chloride, hydrazine hydrate, diethyl ether, benzene, and *N, N*-dimethylformamide (DMF) were purchased from Rankem chemicals. 5-amino tetrazole was purchased from the Aldrich Chemicals. All starting materials were used without further purification. All experimental operations were performed in air.

Synthesis of *N,N*-Dimethylformamide Azine Dihydrochloride (DMAz): 28.6 mL, 0.4 mol of Thionyl chloride (SOCl₂) was added with stirring to DMF (150 mL) at 5 °C. After addition keep this mixture at 5 °C for 24h and then added slowly aqueous hydrazine hydrate (5 mL, 0.1 mol) in 20 ml DMF. After addition the mixture was stirred at room temperature for 48h and the white precipitate of *N, N*-dimethylformamide azine dihydrochloride was collected by filtration and washed with DMF and diethyl ether: 19.1 gm; mp 251 °C.

FTIR: (KBr 4000-400 cm^{-1}): 3473(s), 3223 (w), 2951(w), 2848(w), 2031(m), 1715(s), 1609(m), 1507(s), 1398(w), 1287(s), 1228(m), 1137(s), 1054(s), 1019(m), 877(m), 672(s), 654(m), 530(m), 496(m).

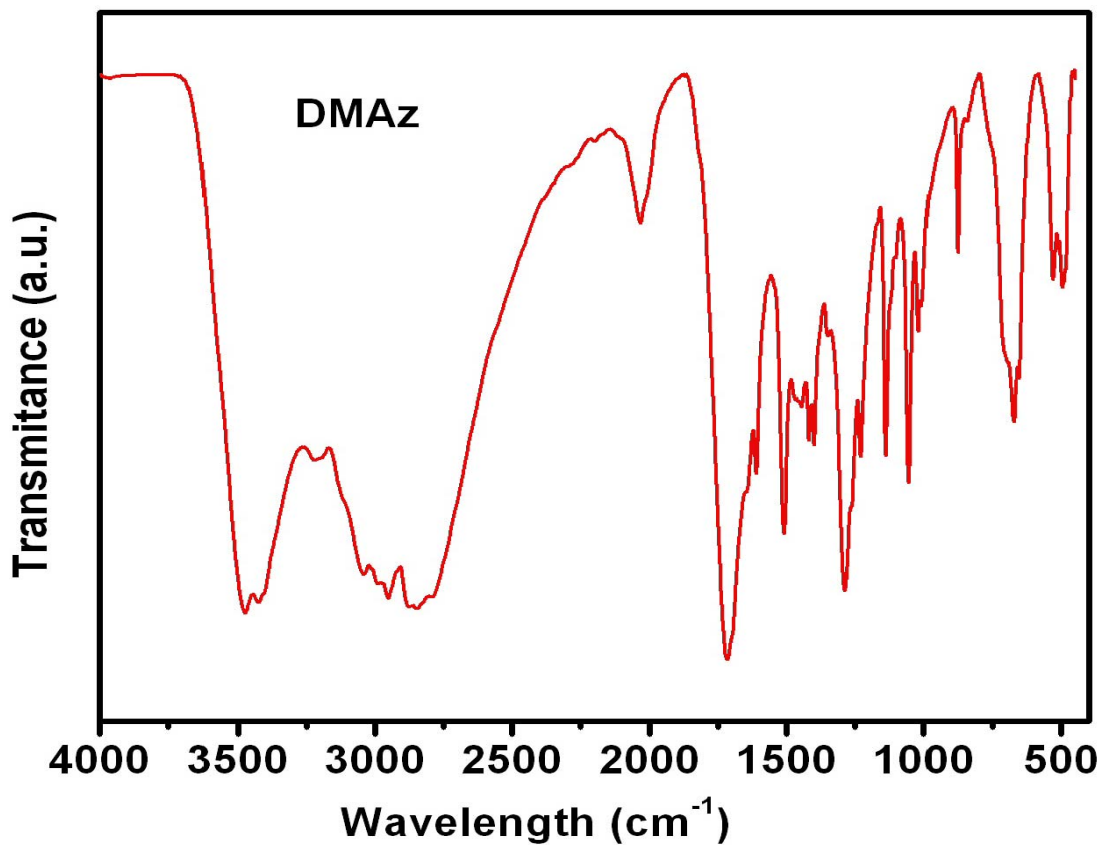
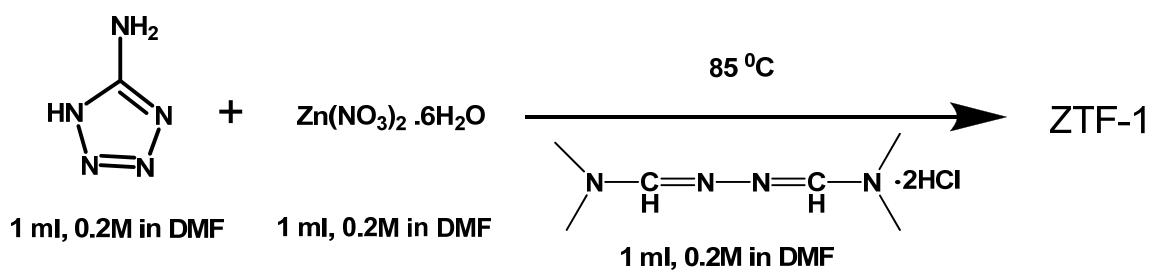


Figure S1. IR data of N,N-dimethylformamide azine dihydrochloride (DMAz).

Synthesis of ZTF-1: 1 ml 0.2(M) DMF solution of *N, N*-dimethylformamide azine dihydrochloride (DMAz) was added to 1 ml 0.2(M) DMF solution of $\text{Zn}(\text{NO}_3)_2 \cdot 6\text{H}_2\text{O}$ and 1 ml 0.2(M) DMF solution of 5-amino Tetrazole in a 5 ml culture tube and heated 90°C temperature for 48h. Colorless crystals were collected by filtration (75% yield by Zn) and washed with DMF and dry acetone then dried in air.



FTIR: (KBr $4000\text{-}400\text{cm}^{-1}$): 3341(s), 3196 (m), 2806(w), 1642(s), 1567(s), 1472(m), 1449(m), 1387(w), 1307(m), 1283(m), 1163(m), 1096(s), 1008(m), 843(m), 750(m), 597(w), 489(s).

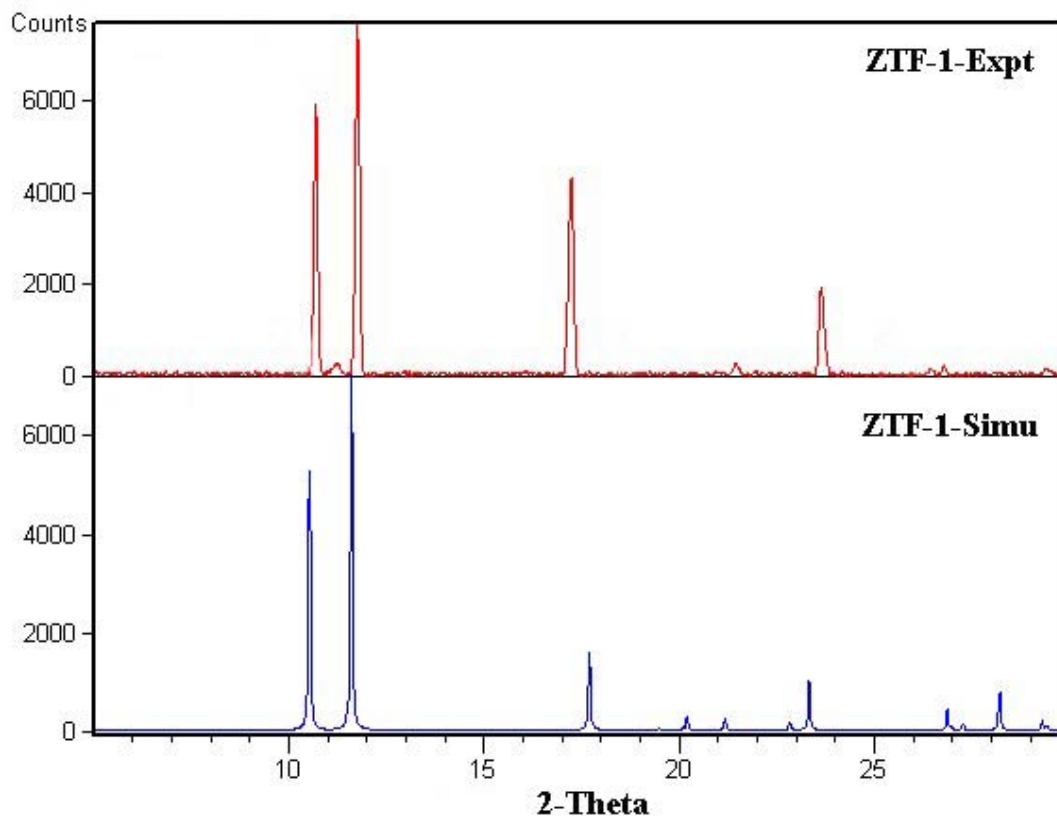


Figure S2. Comparison of the experimental PXRD pattern of as-prepared ZTF-1 (top) with the one simulated from its single crystal structure (bottom).

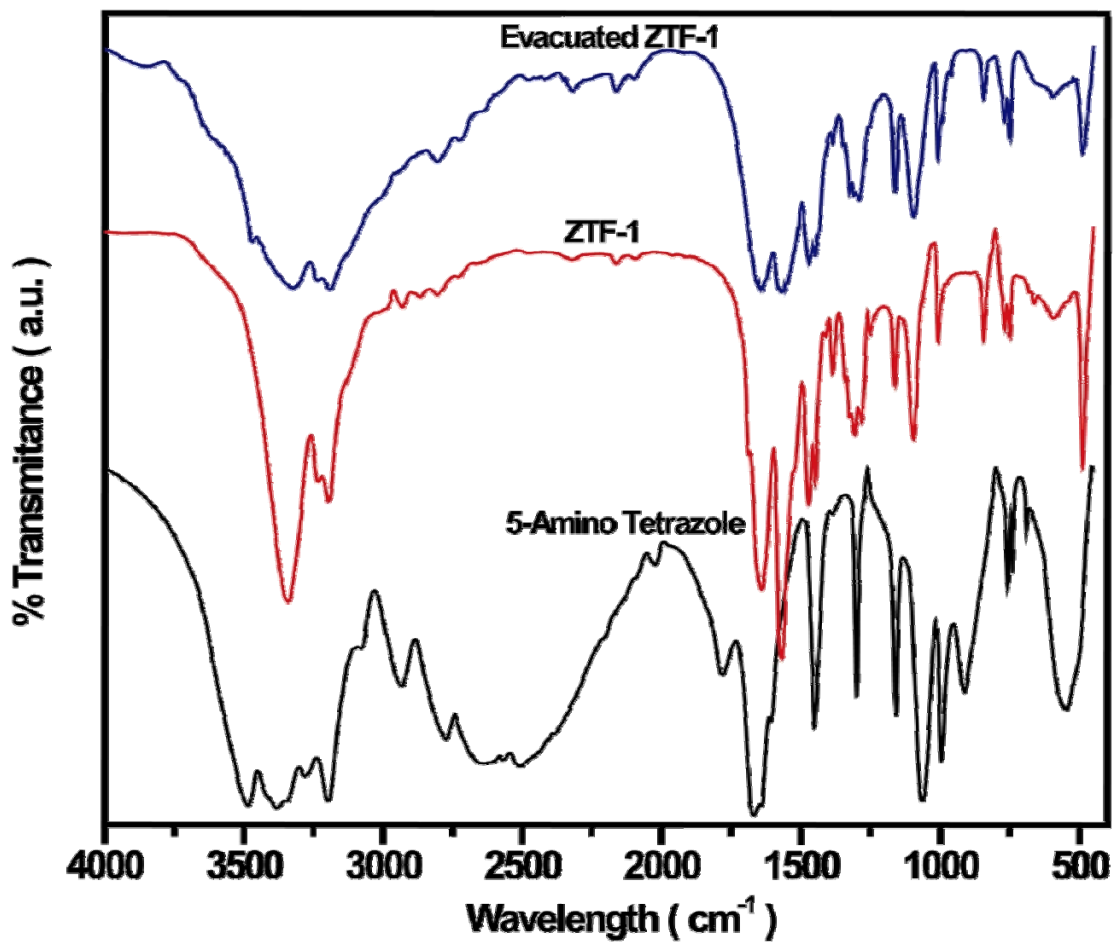
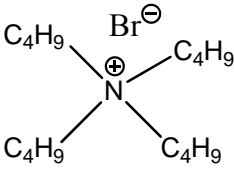
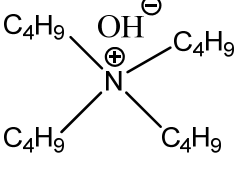
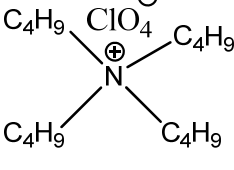
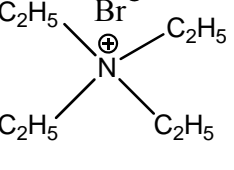
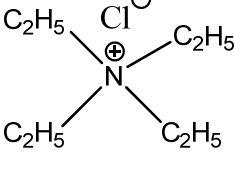
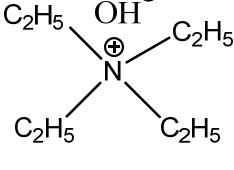
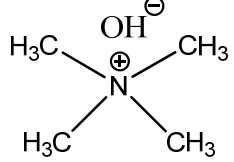
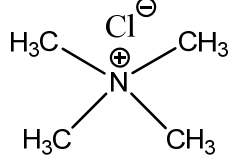
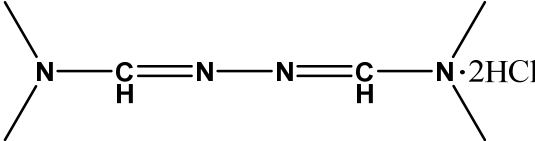


Figure S3. Comparison of the IR data of 5-Amino tetrazole (black, bottom), ZTF-1 (as synthesized, red, middle) and ZTF-1 (evacuated, blue, top). IR stretching indicates the presence of uncoordinated -NH₂ functionality in the MOF.

Table S1. Types of Structure Directing Agents used to Synthesize ZTF-1.

Sl. No	Type of SDA	No Reaction	Unreacted starting material	Crystalline ZTF-1
1		√		
2		√		
3		√		
4		√		
5			√	
6		√		

7			√	
8			√	
9				√

No reaction = after reaction solution is crystal clear.

Unreacted starting Material = after reaction starting material is precipitate.

Section S2. Single crystal X-ray diffraction data collection, structure solution and refinement procedures.

General Data Collection and Refinement Procedures:

All single crystal data were collected on a Bruker SMART APEX three circle diffractometer equipped with a CCD area detector and operated at 1500 W power (50 kV, 30 mA) to generate Mo K α radiation ($\lambda=0.71073$ Å). The incident X-ray beam was focused and monochromated using Bruker Excalibur Gobel mirror optics. Crystals of the **ZTF-1** reported in the paper were mounted on nylon CryoLoops (Hampton Research) with Paraton-N (Hampton Research).

Initial scans of each specimen were performed to obtain preliminary unit cell parameters and to assess the mosaicity (breadth of spots between frames) of the crystal to select the required frame width for data collection. In every case frame widths of 0.5° were judged to be appropriate and full hemispheres of data were collected using the *Bruker SMART*¹ software suite. Following data collection, reflections were sampled from all regions of the Ewald sphere to redetermine unit cell parameters for data integration and to check for rotational twinning using *CELL_NOW*². In no data collection was evidence for crystal decay encountered. Following exhaustive review of the collected frames the resolution of the dataset was judged. Data were integrated using Bruker *SAINT*³ software with a narrow frame algorithm and a 0.400 fractional lower limit of average intensity. Data were subsequently corrected for absorption by the program *SADABS*⁴. The space group determinations and tests for merohedral twinning were carried out using *XPREP*³. In all cases, the highest possible space group was chosen.

All structures were solved by direct methods and refined using the *SHELXTL 97*⁵ software suite. Atoms were located from iterative examination of difference F-maps following least squares refinements of the earlier models. Final models were refined anisotropically (if the number of data permitted) until full convergence was achieved. Hydrogen atoms were placed in calculated positions (C-H = 0.93 Å) and included as riding atoms with isotropic displacement parameters 1.2-1.5 times U_{eq} of the attached C atoms. Data were collected at 298(2) K for all the MOF presented in this paper. This lower temperature was considered to be optimal for obtaining the best data. Electron density within void spaces has not been assigned to any guest entity but has been modeled as isolated oxygen and/or carbon atoms. The foremost errors in all the models are thought to lie in the assignment of guest electron density. All structures were examined using the *Adsym* subroutine of PLATON⁷ to assure that no additional symmetry could be applied to the models. All ellipsoids in ORTEP diagrams are displayed at the 50% probability level unless noted otherwise. For all structures we note that elevated R-values are commonly encountered in MOF crystallography for the reasons expressed above by us and by other research groups.⁸⁻¹⁷

A colorless prismatic crystal ($0.20 \times 0.16 \times 0.10 \text{ mm}^3$) of ZTF-1 was placed in a 0.7 mm diameter nylon CryoLoops (Hampton Research) with Paraton-N (Hampton Research). The loop was mounted on a SMART APEX three circle diffractometer. A total of 7544 reflections were collected of which 3042 were unique and 2879 of these were greater than $2\sigma(I)$. The range of θ was from 2.43 to 28.09°. All non-hydrogen atoms were refined anisotropically ZTF-1 contains two 5-amino tetrazole molecule in the asymmetric unit. It should be noted that other supporting characterization data (*vide infra* Section S2) are

consistent with the crystal structure. Final full matrix least-squares refinement on F^2 converged to $R_1 = 0.0510$ and $wR_2 = 0.1283$ (all data) with GOF = 1.051. Table S1 contains crystallographic data for the ZTF-1.

1. Bruker (2005). *APEX2*. Version 5.053. Bruker AXS Inc., Madison, Wisconsin, USA.
2. Sheldrick, G. M. (2004). *CELL_NOW*. University of Göttingen, Germany. Steiner, Th. (1998). *Acta Cryst.* B54, 456–463.
3. Bruker (2004). *SAINTE-Plus* (Version 7.03). Bruker AXS Inc., Madison, Wisconsin, USA.
4. Sheldrick, G. M. (2002). *SADABS* (Version 2.03) and *TWINABS* (Version 1.02). University of Göttingen, Germany.
5. Sheldrick, G. M. (1997). *SHELXS '97* and *SHELXL '97*. University of Göttingen, Germany.
6. WINGX version 1.80.04. Louis Farrugia, University of Glasgow.
7. A. L. Spek (2005) *PLATON, A Multipurpose Crystallographic Tool*, Utrecht University, Utrecht, The Netherlands.
8. Dakin, L. A., Ong P. C., Panek, J. S., Staples, R. J. & Stavropoulos, P. *Organometallics* **19**, 2896-2908 (2000).
9. Noro, S., Kitaura, R., Kondo, M., Kitagawa, S., Ishii, T., Matsuzaka, H. & Yamashita, M. *J. Am. Chem. Soc.* **124**, 2568-2583 (2002).
10. Eddaoudi, M., Kim, J., Vodak, D., Sudik, A., Wachter, J., O'Keeffe, M. & Yaghi, O. M. *Proc. Natl. Acad. Sci. U.S.A.* **99**, 4900-4904 (2002).

11. Heintz, R. A., Zhao, H., Ouyang, X., Grandinetti, G., Cowen, J. & Dunbar, K. R. *Inorg. Chem.* **38**, 144-156 (1999).
12. Biradha, K., Hongo, Y. & Fujita, M. *Angew. Chem. Int. Ed.* **39**, 3843-3845 (2000).
13. Grosshans, P., Jouaiti, A., Hosseini, M. W. & Kyritsakas, N. *New J. Chem, (Nouv. J. Chim.)* **27**, 793-797 (2003).
14. Takeda, N., Umemoto, K., Yamaguchi, K. & Fujita, M. *Nature (London)* **398**, 794-796 (1999).
15. Eddaoudi, M., Kim, J., Rosi, N., Vodak, D., Wachter, J., O'Keeffe, M. & Yaghi, O. *M. Science* **295**, 469-472 (2002).
16. Kesanli, B., Cui, Y., Smith, M. R., Bittner, E. W., Bockrath, B. C. & Lin, W. *Angew. Chem. Int. Ed.* **44**, 72-75 (2005).
17. Cotton, F. A., Lin, C. & Murillo, C. A. *Inorg. Chem.* **40**, 478-484 (2001).

Table S2. Crystal data and structure refinement for ZTF-1

Empirical formula	C ₅ H ₁₀ N ₁₁ O Zn
Formula weight	305.61
Temperature	293(2) K
Wavelength	0.71073 Å
Crystal system	Monoclinic
Space group	<i>Cc</i>
Unit cell dimensions	$a = 13.330(3) \text{ \AA}$ $\alpha = 90^\circ$ $b = 15.327(3) \text{ \AA}$ $\beta = 131.20(2)^\circ$ $c = 8.7796(17) \text{ \AA}$ $\gamma = 90^\circ$
Volume	1349.7(5)
Z	4
Density (calculated)	1.504
Absorption coefficient	1.829
F(000)	620
Crystal size	0.20 × 0.16 × 0.10 mm ³
Theta range for data collection	2.43 – 28.09
Index ranges	-17 ≤ h ≤ 17, -20 ≤ k ≤ 19, -11 ≤ l ≤ 11
Reflections collected	7544
Independent reflections	3042
Completeness to theta = 26.02°	95.7 %
Absorption correction	Semi-empirical from equivalents
Refinement method	Full-matrix least-squares on F ²
Data / restraints / parameters	3042 / 2 / 174
Goodness-of-fit on F²	1.051
Final R indices [I > 2σ(I)]	R ₁ = 0.0510, wR ₂ = 0.1283
R indices (all data)	R ₁ = 0.0531, wR ₂ = 0.1301
Largest diff. peak and hole	1.017 and -0.442 e.Å ⁻³

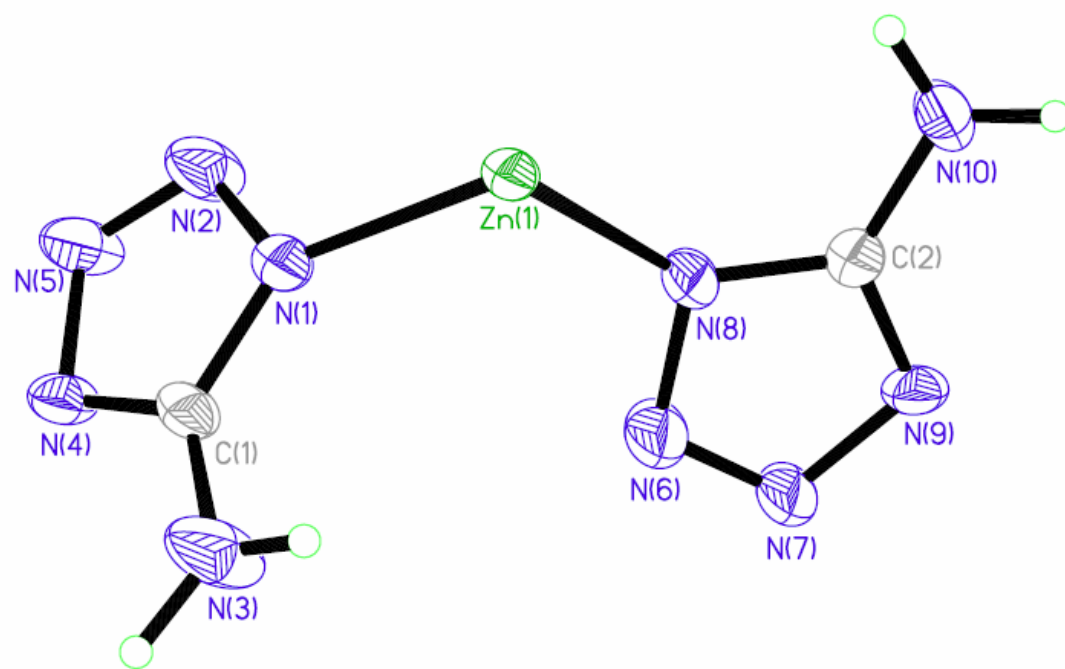


Figure S4. ORTEP drawing of the asymmetric unit of ZTF-1.

Table S3. Types of ZIFs (including the number of times) reported in the literature and the M-X-M bond angle range.

Sl. No	Type	Number of Hits	Angle Range
1	sod	12	143.32 to 147.78
2	dia	10	140.2 to 149.4
3	crb	7	142.44 to 149.62
4	gis	6	142.34 to 149.05
5	rho	5	141.88 to 151.39
6	cag	5	140.84 to 143.31
7	zni	5	142.76 to 146.38
8	mog	4	141.87 to 146.25
9	ita	4	141.43 to 142.22
10	gme	3	144.26 to 146.13
11	neb	3	140.88 to 145.14
12	nog	3	138.28 to 145.88
13	frl	2	144.81 to 149.25
14	dft	2	143.71 to 145.22
15	coi	2	144.46 to 144.49
16	mer	2	144.81 to 145.03
17	zec	1	142.23
18	zeb	1	140.18
19	fes	1	146.81
20	ana	1	144.88
21	srs-c-b	1	144.16

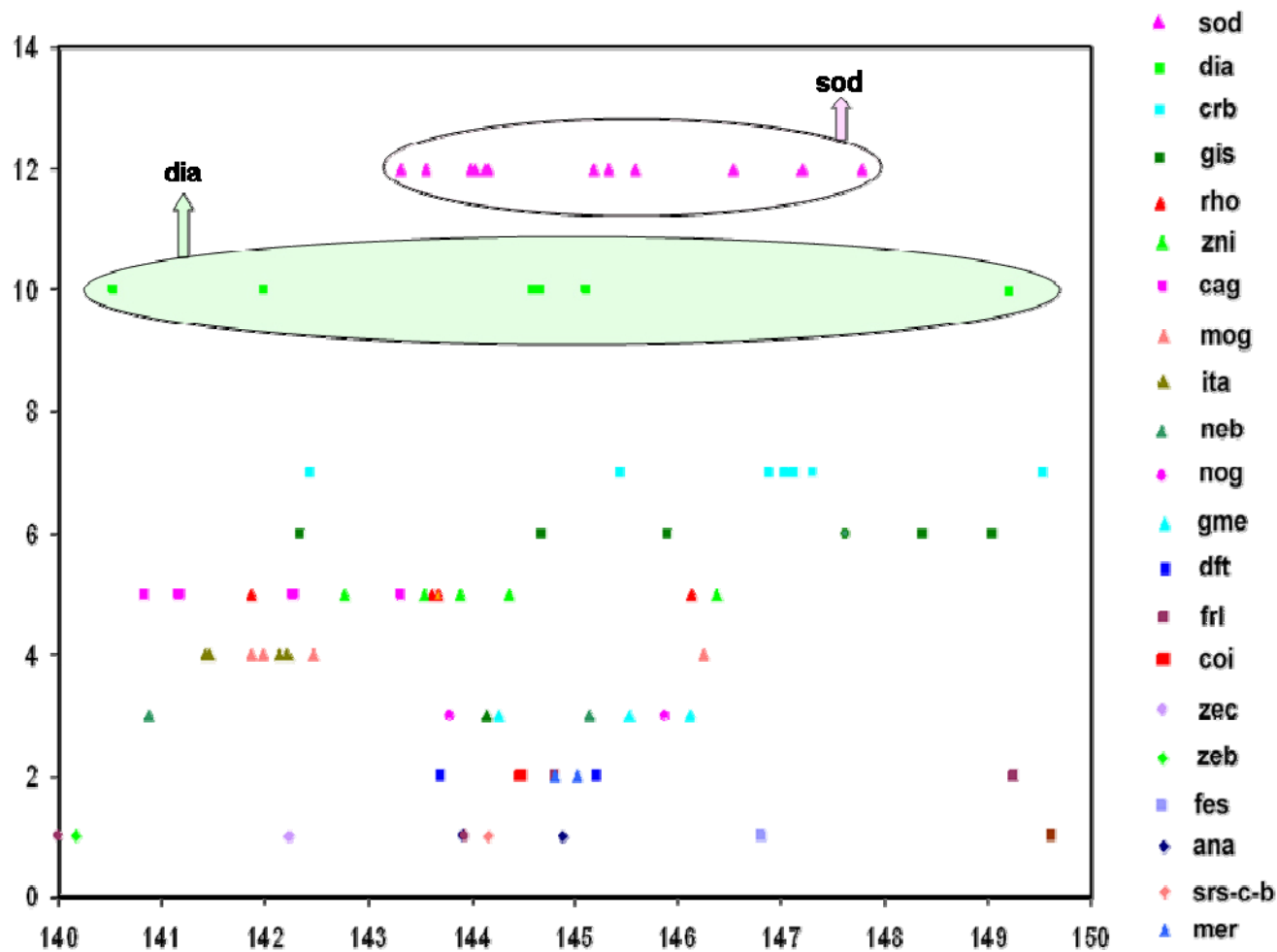


Figure S5. Angular distribution figure for the M-X-M angles. X axis represent the angle range and Y axis represent the number of hits. It is to be noted that we have assigned total number of hits for every case in order to separate each type from other.

Section S3. Thermal stability of ZTF-1

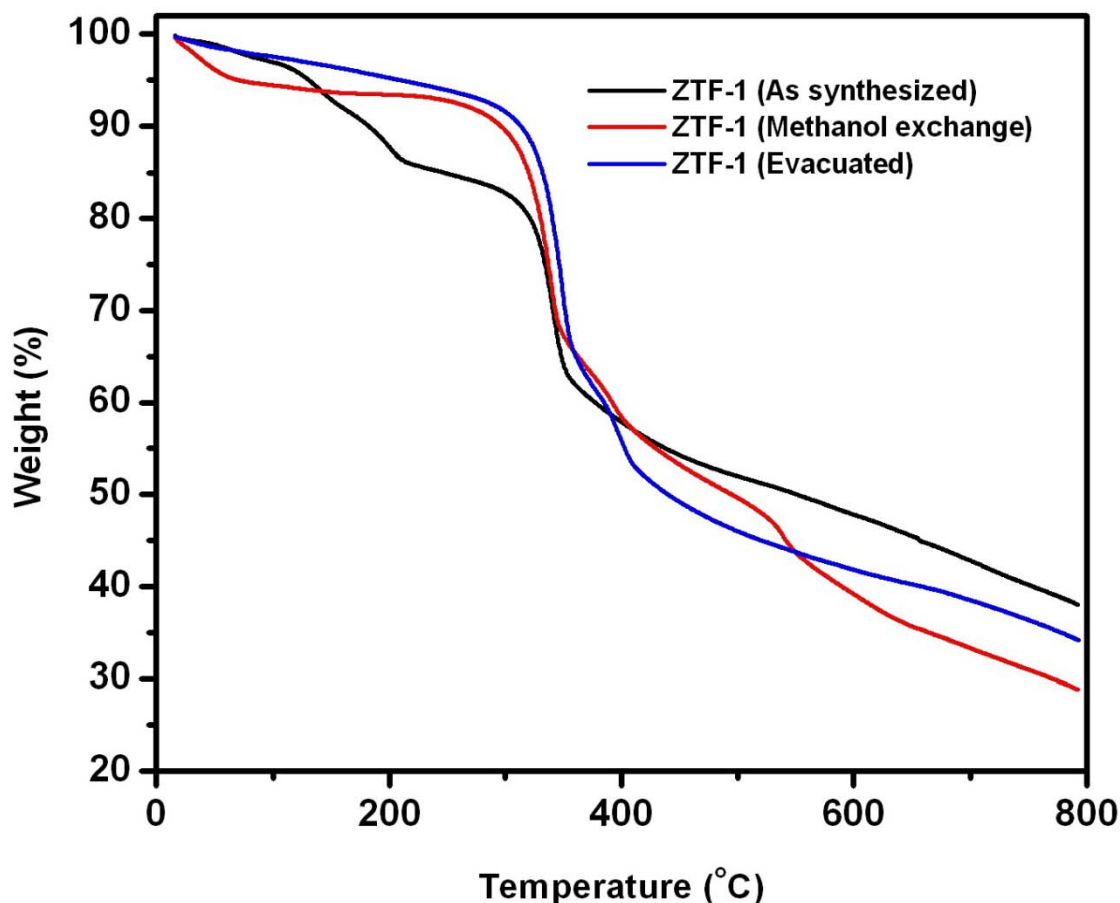


Figure S6. Overlay of TGA traces of as-synthesized (black), solvent-exchanged (red), and activated (blue) samples of ZTF-1.

TGA traces of as-synthesized, methanol-exchanged, and activated ZTF-1 are shown in Figure S6. In the TGA trace of methanol-exchanged ZTF-1 sample, the original gradual weight-loss step of 16.6% up to 204 °C was replaced by a small initial step (6.1%) at 100 °C temperature, a plateau until 380 °C, and a sharp weight loss from that point onward, indicating decomposition of the material. The sample was activated by heating at 85 °C under vacuum for 72 hours. A flat plateau to 380 °C and a subsequent decomposition of the material indicates the activation of the sample was complete. The loss of weight (< 4%) at low temperature could be due to removal of adhered moisture.

Section S4. Gas Adsorption analysis of ZTF-1.

Table S4. Lists of high CO₂ uptake of different MOFs reported in the literature.

SL. No.	MOFs	CO ₂ uptake mmol/g at 1 bar		Reference
		273K	298K	
1	Mg\DOBDC		8.08	S. R. Caskey, A. G. Wong-Foy, A. J. Matzger, <i>J. Am. Chem. Soc.</i> 2008, 130 , 10870.
2	Co\DOBDC		7.1	S. R. Caskey, A. G. Wong-Foy, A. J. Matzger, <i>J. Am. Chem. Soc.</i> 2008, 130 , 10870.
3	Ni\DOBDC		5.8	S. R. Caskey, A. G. Wong-Foy, A. J. Matzger, <i>J. Am. Chem. Soc.</i> 2008, 130 , 10870.
4	Zn\DOBDC		5.5	S. R. Caskey, A. G. Wong-Foy, A. J. Matzger, <i>J. Am. Chem. Soc.</i> 2008, 130 , 10870.
5	HKUST-1 (295 K)		4.7	Q. M. Wang, D. Shen, M. Bulow, M. L. Lau, S. Deng, F.R. Fitch, N. O. Lemcoff, J. Semanscin, <i>Microporous and Mesoporous Materials.</i> 2002, 55 , 217
6	Zn + 4,4' bipy + (BTA-TBA)		4.1	O. K. Farha. C. D. Malliakas, M. G. Kanatzidis, J. T. Hupp, <i>J. Am. Chem. Soc.</i> 2010, 132 , 950.
7	[Zn ₃ (OH)(<i>p</i> -CDC) _{2.5}] _n		4.004	Y. S. Bae, O. K. Farha, A. M. Spokoyny, C. A. Mirkin, J. T. Hupp, R. Q. Snurr, <i>Chem. Commun.</i> , 2008, 4135
8	Bio MOF 11	6.0	4.0	J. An, S. J. Geib, N. L. Rosi <i>J. Am. Chem. Soc.</i> 2010, 132 , 38
9	ZTF-1	5.35	3.79	
10	Zn ₂ (C ₂ O ₄)(C ₂ N ₄ H ₃) ₂ .(H ₂ O) _{0.5}	4.30	3.78	R. Vaidhyathan, S. S. Iremonger, K. W. Dawson, G. K. H. Shimizu, <i>Chem. Commun.</i> , 2009, 5230
11	UMCM-150		2.8	A. G. Wong-Foy, O. Lebel, A. J. Matzger <i>J. Am. Chem. Soc.</i> 2007, 129 , 15740.

12	TMA@ Bio-MOF-1,	4.5		J. An and N. L. Rosi, <i>J. Am. Chem. Soc.</i> 2010, 132 , 5578.
13	TEA@ Bio-MOF-1	4.2		J. An and N. L. Rosi, <i>J. Am. Chem. Soc.</i> 2010, 132 , 5578.
14	TBA@ Bio-MOF-1 and Bio-MOF-1	3.5		J. An and N. L. Rosi, <i>J. Am. Chem. Soc.</i> 2010, 132 , 5578.
15	ZIF-78	3.348	2.23	R. Banerjee, H. Furukawa, D. Britt, C. Knobler, M. O'Keeffe, O. M. Yaghi, <i>J. Am. Chem. Soc.</i> 2009, 131 , 3875.
16	ZIF-96		2.16	W. Morris, B. Leung, H. Furukawa, O. K. Yaghi,† N. He, H. Hayashi, Y. Houndonougbo, M. Asta, B. B. Laird, O. M. Yaghi, <i>J. Am. Chem. Soc.</i> 2010, 132 , 11006.
16	IMOF-3(C ₆ H ₆ N ₄ O ₂ Zn)		2.14	F. Debatin, A. Thomas, A. Kelling, N. Hedin, Z. Bacsik, I. Senkovska, S. Kaskel, M. Junginger, H. Muller, U. Schilde, C. Jager, A. Friedrich, H. J. Holdt <i>Angew. Chem. Int. Ed.</i> 2010, 49 , 1258
17	ZIF-69	3.03	1.69	R. Banerjee, H. Furukawa, D. Britt, C. Knobler, M. O'Keeffe, O. M. Yaghi, <i>J. Am. Chem. Soc.</i> 2009, 131 , 3875.

Gas Adsorption analysis of ZTF-1

All low-pressure gas-sorption experiments (up to 1 atm) were performed on a Quantachrome Autosorb-1 automatic volumetric instrument. The as-synthesized ZTF-1 samples were immersed in dry methanol at ambient temperature for 72 h, evacuated at ambient temperature for 24 h, then at an elevated temperature (85 °C) for 48 h. The architectural rigidity and consequently the permanent porosity of evacuated ZTF-1 was unequivocally proven by gas-sorption analysis. Type I nitrogen adsorption isotherm

behavior was observed for these ZTF-1 (Fig.S7), which reveals its microporous nature. Apparent surface areas of $443.8 \text{ m}^2 \text{ g}^{-1}$ (Langmuir model, $P/P_0 = 0.06\text{--}0.30$, the linearity of fitting 0.999) and $355.3 \text{ m}^2 \text{ g}^{-1}$ (Brunauer– Emmett–Teller (BET) model [K. S. Walton, R. Q. Snurr, *JACS* **129**, 8552 (2007)], $P/P_0 = 0.03\text{--}0.06$, the linearity of fitting 0.99) for ZTF-1 were obtained by using the data points on the adsorption branch.

N₂ adsorption isotherm for ZTF-1.

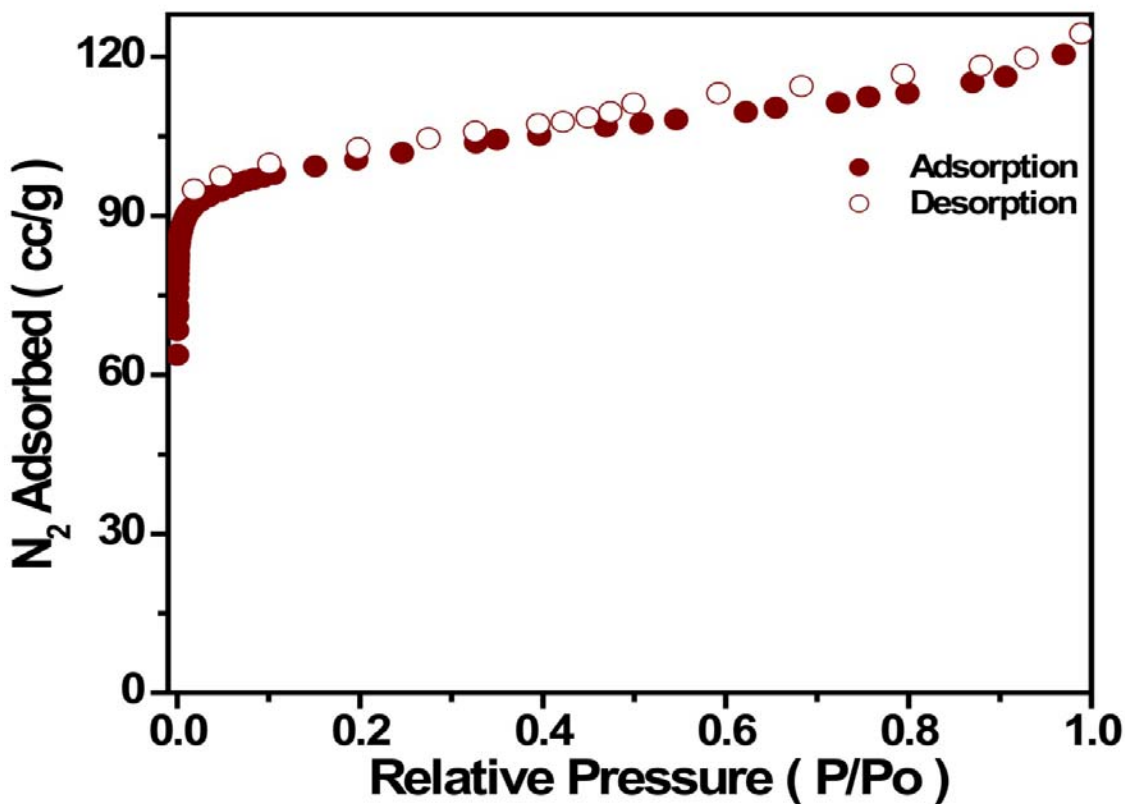


Figure S7. The N₂ gas-sorption isotherms for ZTF-1 measured at 77 K. The filled and open circles represent adsorption and desorption branches, respectively.

Selective CO₂ adsorption over N₂ for ZTF-1 at 273 K.

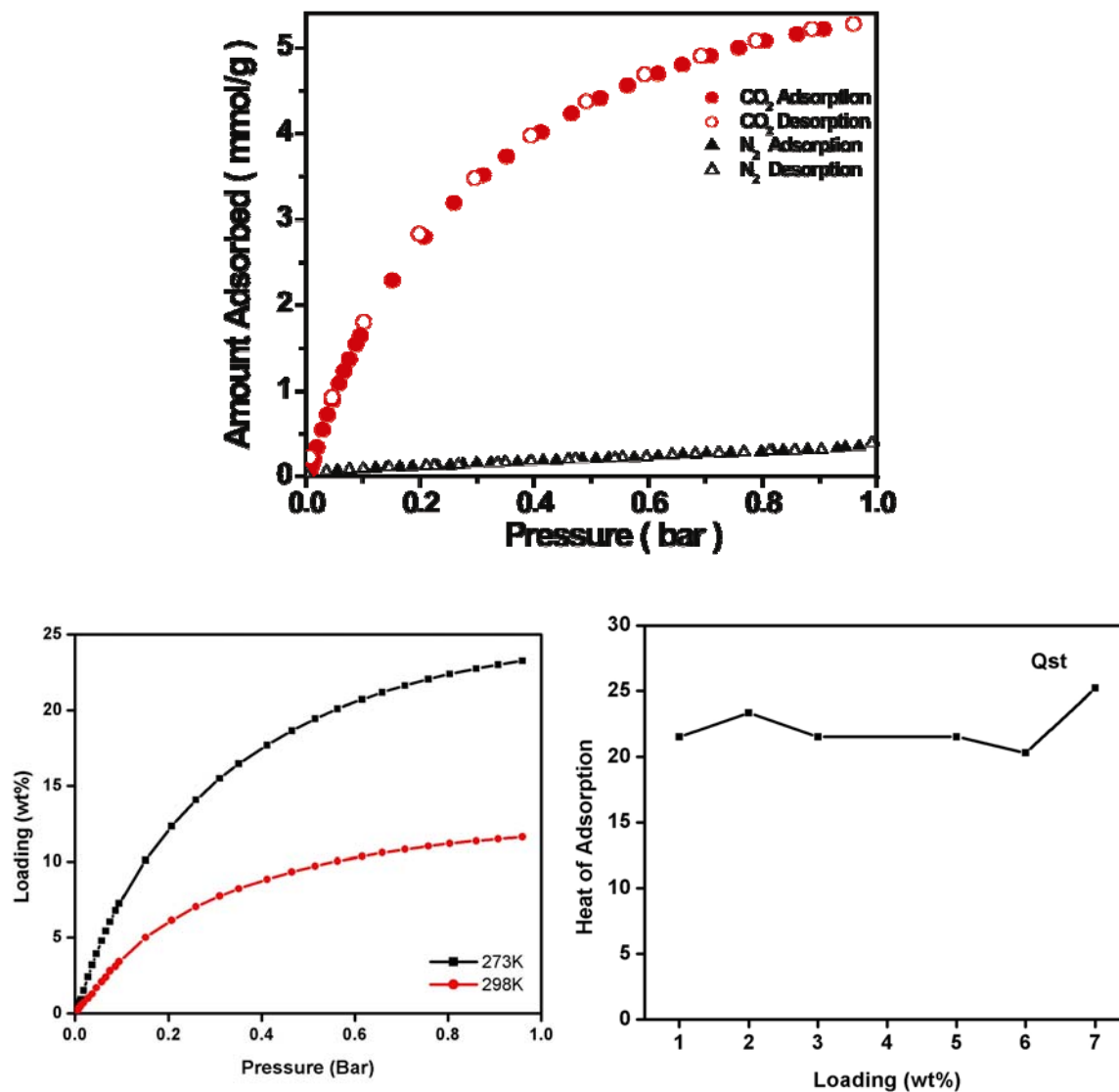


Figure S8. CO₂ (circles) and N₂ (triangles) adsorption isotherm at 273K of ZTF-1. CO₂ adsorption at 273 and 298K for ZTF-1. The corresponding Qst value for the CO₂ adsorption has also been plotted. Filled and open symbols represent adsorption and desorption branches.

H₂ adsorption isotherm for ZTF-1.

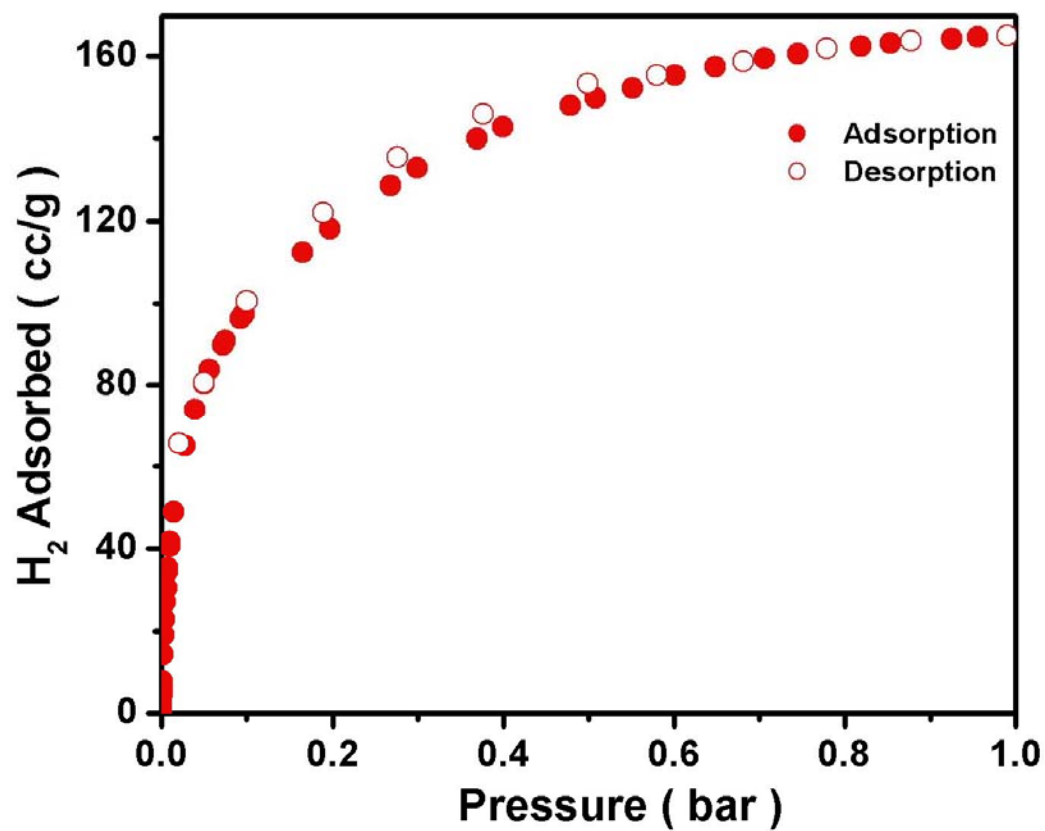


Figure S9. H₂ adsorption isotherm for ZTF-1 taken at 77 K (blue). Filled and open symbols represent adsorption and desorption branches.

The repeatability of the H₂ adsorption behavior

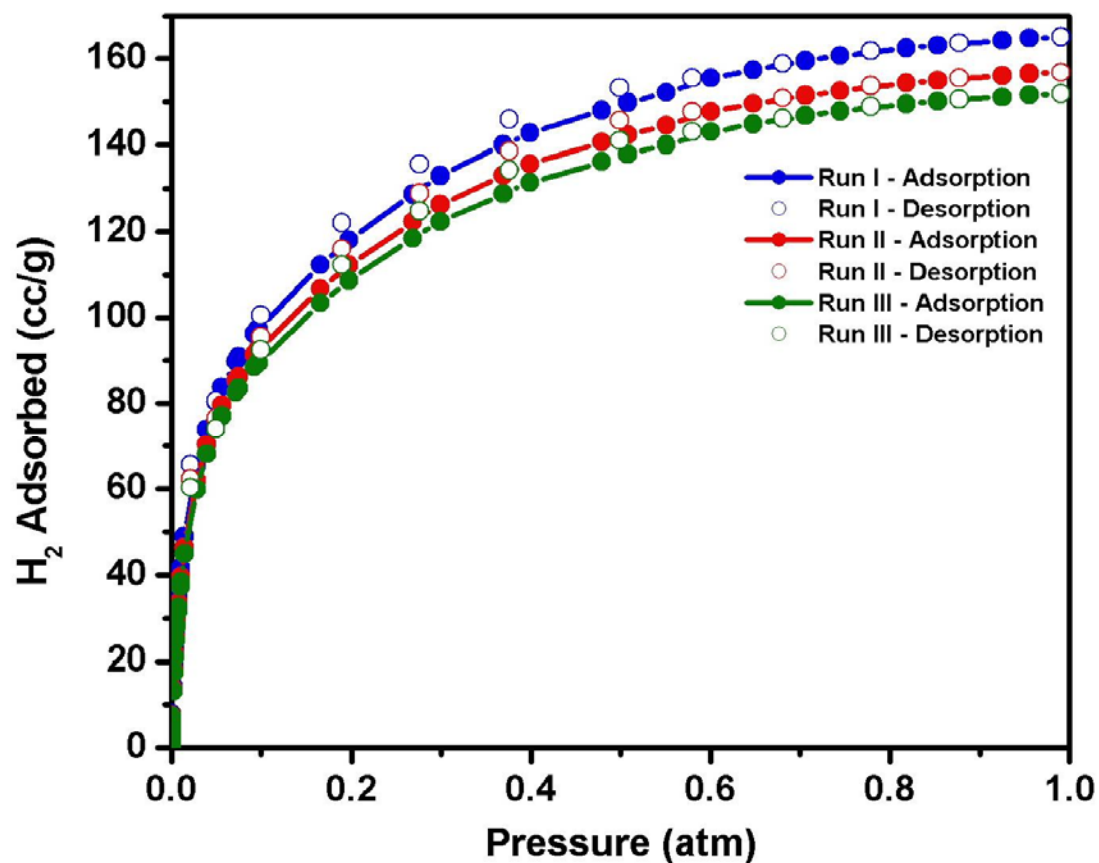


Figure S10. The repeatability of the H₂ adsorption behavior was confirmed by reproducing the same isotherm three times at 77 K. Blue first time; red second time; green third time. Filled and open symbols represent adsorption and desorption branches. Connecting traces are guides for eye.

Section S5. Computational Studies for ZTF-1:

1. Simulation Model and Method

The crystal structure of ZTF-1 measured from experiment was used in simulation. Figure S11 shows the morphology and diameter of the pore along the X direction calculated using HOLE program.¹ The pore diameter ranges from 4.50 to 4.85 Å. The porosity of ZTF-1 is 0.626, evaluated using Materials Studio² with a Connolly probe radius equal to zero.

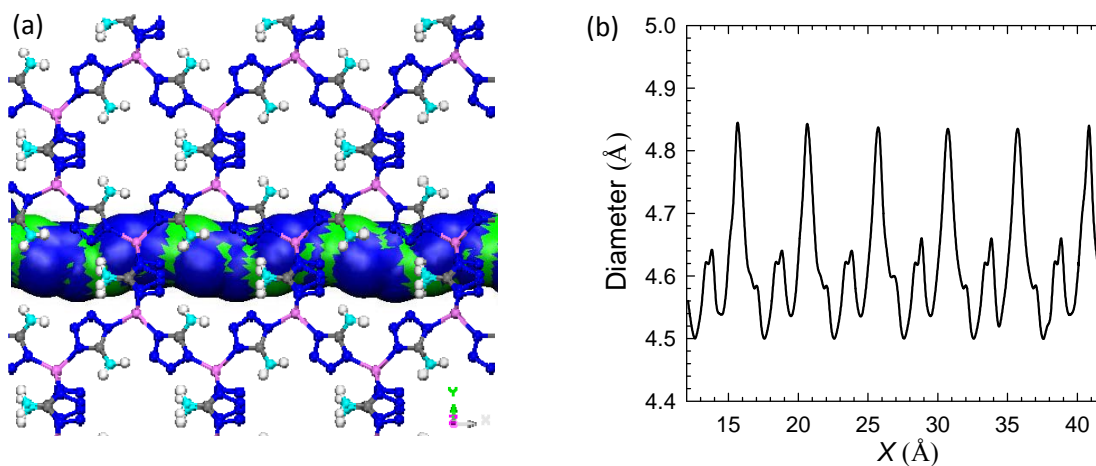


Figure S11. Pore morphology and diameter along the X axis in ZTF-1.

The atomic charges of the framework atoms in a unit cell of ZTF-1 were calculated from density functional theory (DFT) in Materials Studio.² The DFT calculation used the Becke exchange plus Lee-Yang-Parr correlation functional and the all-electron core potentials. The double- ξ numerical polarization (DNP) basis set was adopted, which is comparable to the 6-31G(d,p) Gaussian-type basis set. Mulliken population analysis was used to estimate the atomic charges as listed in Table S5.

Table S5. Atomic charges in ZTF-1 with the atomic labels indicated in Figure S12.

Atom type	N1	N2	N3	Zn	C	H
Charge	-0.064	-0.458	-0.091	0.969	0.473	0.101

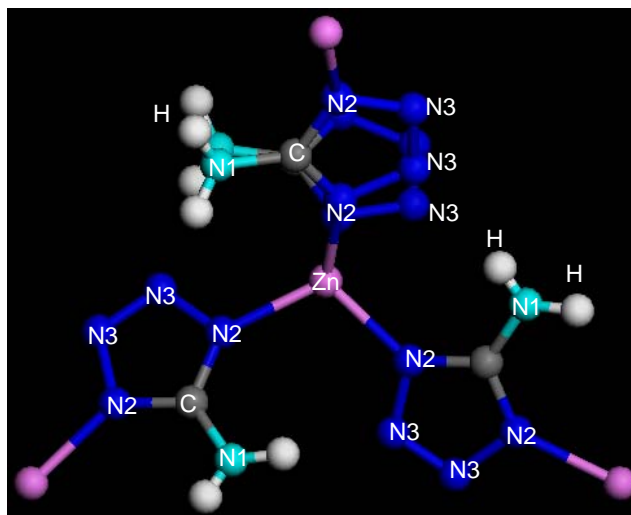


Figure S12. Atomic labels of ZTF-1.

CO₂ was represented as a three-site rigid molecule and its intrinsic quadrupole moment was described by a partial-charge model³. The partial charges on C and O atoms were $q_C = 0.576e$ and $q_O = -0.288e$ ($e = 1.6022 \times 10^{-19}$ is the elementary charge). The C–O bond length was 1.18 Å and the bond angle O–C–O was 180°. The LJ parameters for CO₂ were $\sigma_C = 2.789$ Å, $\varepsilon_C = 29.66$ K, $\sigma_O = 3.011$ Å, $\varepsilon_O = 82.96$ K. The dispersion interactions of the framework atoms in ZTF-1 were modeled by the Universal Force Field (UFF).⁴ The Lorentz-Berthelot combining rules were used to calculate the cross LJ interaction parameters. A number of simulation studies have shown that UFF can accurately predict gas adsorption in various MOFs.⁵⁻⁸

CO₂ adsorption in ZTF-1 was simulated by grand-canonical Monte Carlo (GCMC) simulation in Materials Studio.² The framework and individual CO₂ molecules were treated as rigid. The LJ interactions were evaluated using a spherical cutoff of 12.5 Å and the electrostatic interactions were calculated using the Ewald summation with a precision of 10⁻⁵ kcal/mol. Two types of trial moves were conducted for CO₂ molecules, namely, translation and rotation. The number of steps in the simulation was 2 × 10⁶ for equilibration and 10⁷ for production.

2. Simulation Results and Discussion

Figure S13(a) shows the adsorption isotherm of CO₂ in ZTF-1 at 273 K. The simulated isotherm agrees quite well with experiment. The capacity of CO₂ at 100 kPa is about 5.3 mmol/g at 273 K, which is higher than in most MOFs (MOF-2, MOF-177, MOF-505, IRMOF-1, -3, -6 and -11).⁹ The high CO₂ capacity is attributed to the narrow pores in ZTF-1 and the presence of uncoordinated tetrazolate nitrogen and free -NH₂. As a consequence, there is a substantial overlap of the potential fields for CO₂ in the pores, and a strong interaction between CO₂ and the framework. Figure S13(b) shows the calculated isosteric heat Q_{st} for CO₂ adsorption in ZTF-1. Q_{st} increases with increasing loading, which is similar to CO₂ adsorption in IRMOF-1.⁸ The increase of Q_{st} is due to the cooperative attractive interactions between adsorbed CO₂ molecules. However, the magnitude of Q_{st} in ZTF-1 is much higher than in IRMOF-1. It should be noted that possible coordinative interactions between CO₂ and the nitrogen atoms in ZTF-1 were not taken into account in the GCMC simulation; consequently, the calculated Q_{st} particularly at low loadings might be underestimated. More accurate calculations are currently underway using *ab initio* method.

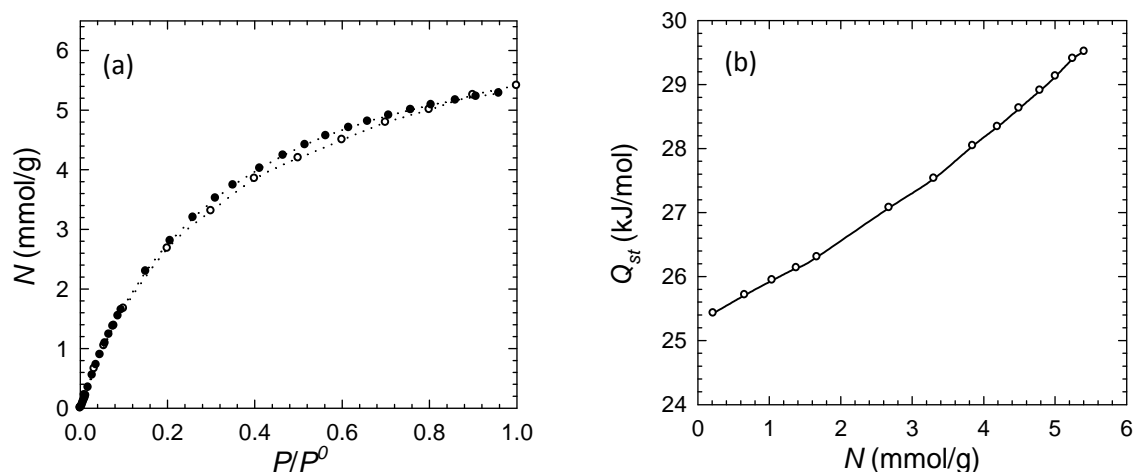


Figure S13. (a) Isotherm and (b) isosteric heat for CO₂ adsorption in ZTF-1 at 273 K. The open symbols are from simulation and the filled symbols are from experiment.

To identify the favorable binding sites for CO₂ in ZTF-1, Figure S14 shows the density distributions of adsorbed CO₂ molecules along the *YZ* and *XY* planes at 273 K and 100 kPa. We see that CO₂ molecules are primarily adsorbed in the pores along the *X* axis and the binding sites are mostly located in the pore centers. To better understand the nature of the binding sites, Figure S15(a) shows the distances between a single CO₂ molecule and the uncoordinated tetrazolate/amino nitrogen atoms in a 6-membered ring that consists of Zn atoms. It is observed that CO₂ is closer to the uncoordinated tetrazolate nitrogen compared to the amino nitrogen. The observed different distances can be further elucidated from the radial distribution functions $g(r)$ of CO₂ around nitrogen atoms. The $g(r)$ was calculated by

$$g_{ij}(r) = \frac{\Delta N_{ij} V}{4\pi r^2 \Delta r N_i N_j}$$

where r is the distance between species i and j , ΔN_{ij} is the number of species j around i within a shell from r to $r + \Delta r$, V is the volume, N_i and N_j are the numbers of species i

and *j*. As shown in Figure S15(b), a pronounced peak is observed at $r = 3.5$ Å in the $g(r)$ around N3 and at $r = 4.0$ Å in the $g(r)$ around N1. This analysis reveals that CO₂ is more preferentially bound onto the uncoordinated tetrazolate nitrogen than the amino nitrogen.

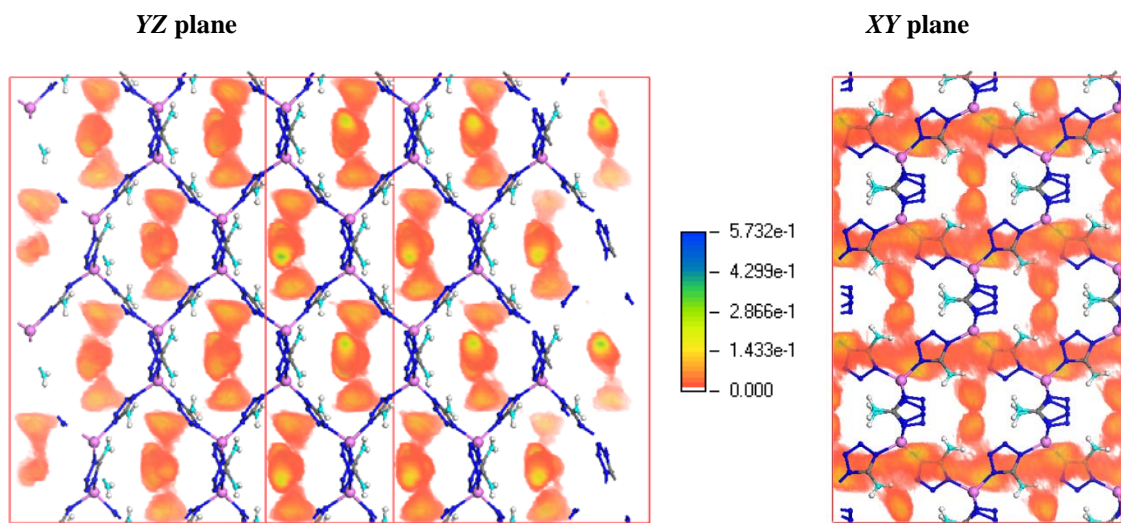


Figure S14. Density distributions of adsorbed CO₂ molecules on (a) YZ and (b) XY planes in ZTF-1 at 273 K and 100 kPa.

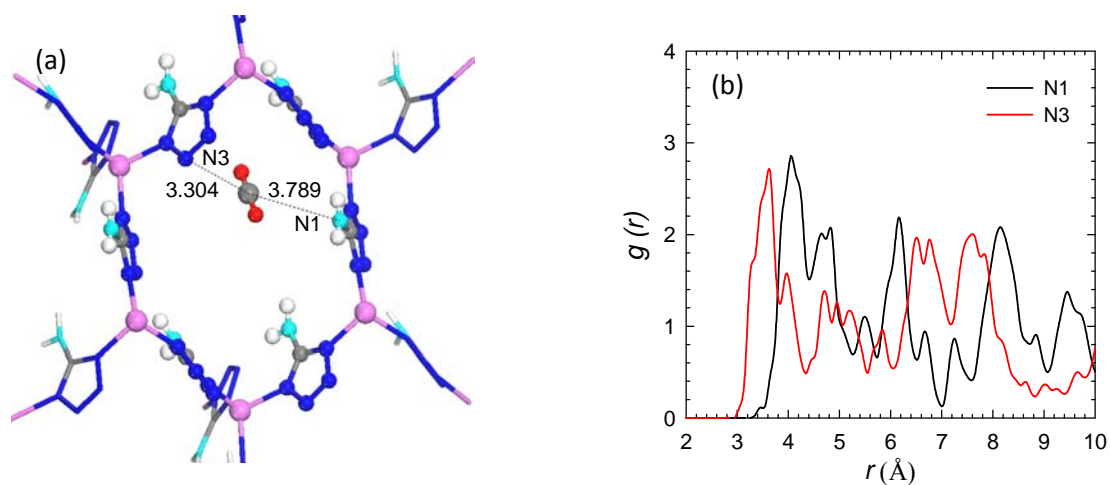


Figure S15. (a) Distances and (b) radial distribution functions between a single CO₂ molecule and the uncoordinated tetrazolate (N3) /amino (N1) nitrogen atoms at 273 K.

To further elucidate the role of the uncoordinated tetrazolate nitrogen and amino nitrogen, we identified the binding sites and energies between CO₂ and different organic linkers from the first-principles method. Fig. S16 illustrates three organic linkers; (a) is the original linker in ZTF-1, (b) and (c) are two analogues. There is no amino group in (b) and no uncoordinated tetrazolate nitrogen in (c). The second-order Møller-Plesset (MP2) method was used in the first-principles calculations by Gaussian 03 program.⁹ The structure optimization between CO₂ and each linker was performed with 6-31++G** basis set, and the energy was calculated with 6-311++G** basis set. The basis set superposition error (BSSE) was corrected by the counterpoise method.¹⁰

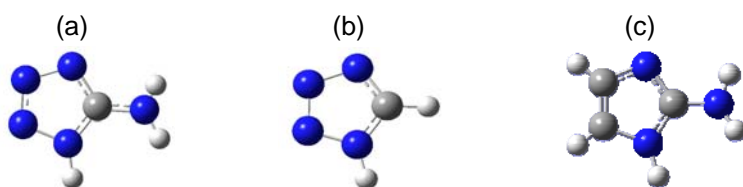


Figure S16. Organic linkers (a) CN₅H₃ in ZTF-1, (b) CN₄H₂ and (c) C₃N₃H₅.

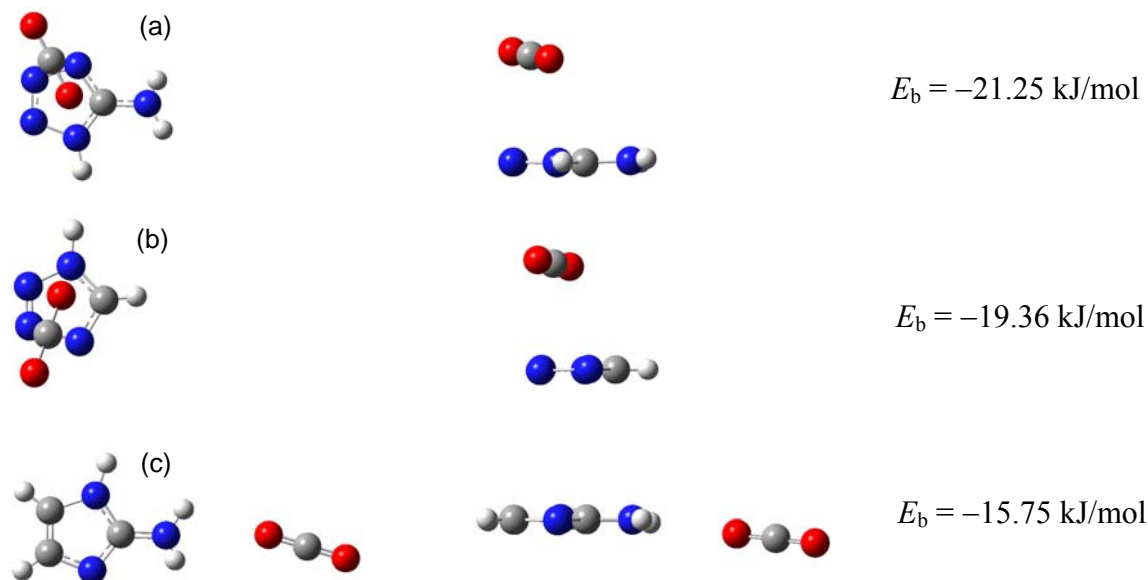


Figure S17. Optimized structures (top and side views) and binding energies of CO₂ with (a) CN₅H₃, (b) CN₄H₂ and (c) C₃N₃H₅.

Fig. S17 shows the optimized structures and binding energies of CO₂ with (a) CN₅H₃ in ZTF-1, (b) CN₄H₂ and (c) C₃N₃H₅. The binding energy of CO₂ is the strongest with linker (a), followed by (b) and (c). In addition, the optimized structure for CO₂ with (a) is closer to the uncoordinated tetrazolate nitrogen than the amino nitrogen. This reveals that the uncoordinated tetrazolate nitrogen is a more favorable site for CO₂, which is consistent with that found by the GCMC simulation.

References:

- (1) Smart, O. S.; Neduvellil, J. G.; Wang, X.; Wallace, B. A.; Sansom, M. S. P., *J. Mol. Graphics Model.* 1996, *14*, 354.
- (2) Materials Studio, v., Accelrys: San Diego, 2007.
- (3) Hirotsu, A.; Mizukami, K.; Miura, R.; Takaba, H.; Miya, T.; Fahmi, A.; Stirling, A.; Kubo, M.; Miyamoto, A., *Appl. Surf. Sci.* 1997, *120*, 81.
- (4) Rappe, A. K.; Casewit, C. J.; Colwell, K. S.; Goddard, W. A.; Skiff, W. M., *J. Am. Chem. Soc.* 1992, *114*, 10024.
- (5) Garberoglio, G.; Skoulidas, A. I.; Johnson, J. K., *J. Phys. Chem. B.* 2005, *109*, 13094.
- (6) Skoulidas, A. I.; Sholl, D. S., *J. Phys. Chem. B.* 2005, *109*, 15760.
- (7) Babarao, R.; Hu, Z. Q.; Jiang, J. W.; Chempath, S.; Sandler, S. I., *Langmuir* 2007, *23*, 659.
- (8) Babarao, R.; Jiang, J. W., *Langmuir* 2008, *24*, 6270.
- (9) Frisch, M. J.; Trucks, G. W.; Schlegel, H. B.; Scuseria, G. E.; Robb, M. A.; Cheeseman, J. R.; Zakrzewski, V. G.; Montgomery, J. A.; Stratmann, R. E.; Burant, J. C.; Dapprich, S.; Millam, J. M.; Daniels, A. D.; Kudin, K. N.; Strain, M. C.; Farkas, O.; Tomasi, J.; Barone, V.; Cossi, M.; Cammi, R.; Mennucci, B.; Pomelli, C.; Adamo, C.; Clifford, S.; Ochterski, J.; Petersson, G. A.; Ayala, P. Y.; Cui, Q.; Morokuma, K.; Malick, D. K.; Rabuck, A. D.; Raghavachari, K.; Foresman, J. B.; Cioslowski, J.; Ortiz, J. V.; Stefanov, B. B.; Liu, G.; Liashenko, A.; Piskorz, P.; Komaromi, I.; Gomperts, R.; Martin, R. L.; Fox, D. J.; Keith, T.; Al-Laham, M. A.; Peng, C. Y.; Nanayakkara, A.; Gonzalez, C.; Challacombe, M.; Gill, P. M. W.; Johnson, B. G.; Chen, W.; Wong, M. W.; Andres, J. L.; Head-Gordon, M.; Replogle, E. S.; Pople, J. A. *Gaussian 03*, Revision D.01 ed.; Gaussian, Inc.: Wallingford CT, 2004.
- (10) Boys, S. F.; Bernardi, F., *Mol. Phys.*, 1970, *19*, 553.